ACS OMEGA

Open Access

http://pubs.acs.org/journal/acsodf

Article

Binding Modes of Carnostatine, Homocarnosine, and Ophidine to Human Carnosinase 1

Borvornwat Toviwek, Thanathip Suwanasopee, Skorn Koonawootrittriron, Danai Jattawa, and Prapasiri Pongprayoon*

Cite This: *ACS Omega* 2023, 8, 42966−42975

Read Online

ACCESS | Metrics & More | Article Recommendations | Supporting Information

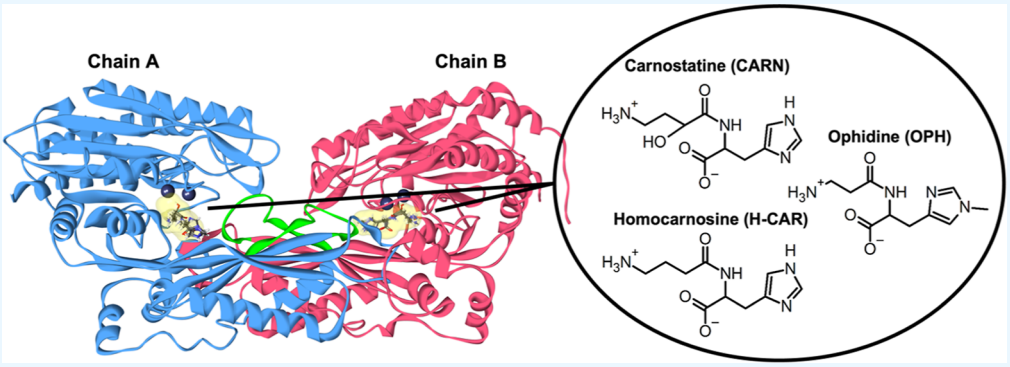

ABSTRACT: Carnosine (CAR), anserine (ANS), homocarnosine (H-CAR), and ophidine (OPH) are histidine-containing dipeptides that show a wide range of therapeutic properties. With their potential physiological effects, these bioactive dipeptides are considered as bioactive food components. However, such dipeptides display low stability due to their rapid degradation by human serum carnosinase 1 (CN1). A dimeric CN1 hydrolyzes such histidine-containing compounds with different degrees of reactivities. A selective CN inhibitor, carnostatine (CARN), was reported to effectively inhibit CN's activity. To date, the binding mechanisms of CAR and ANS have been recently reported, while no clear information about H-CAR, OPH, and CARN binding is available. Thus, in this work, molecular dynamics simulations were employed to elucidate the binding mechanism of H-CAR, OPH, and CARN. Among all, the amine end and imidazole ring are the main players for trapping all of the ligands in a pocket. OPH shows the poorest binding affinity, while CARN displays the tightest binding. Such firm binding is due to the longer amine chain and the additional hydroxyl (−OH) group of CARN. H-CAR and CARN are analogous, but the absence of the −OH moiety in H-CAR significantly enhances its mobility, resulting in the reduction in binding affinity. For OPH which is an ANS analogue, the methylated imidazole ring destroys the OPH−CN1 interaction network at this region, consequentially leading to the poor binding ability. An insight into how CN recognizes and binds its substrates obtained here will be useful for designing an effective strategy to prolong the lifetime of CAR and its analogues after ingestion.

INTRODUCTION

Carnosine (CAR), anserine (ANS), homocarnosine (H-CAR), and ophidine (OPH) are histidine-containing dipeptides. These compounds show a wide range of therapeutic properties. Especially, CAR and ANS play an important role in muscular function,[1] homeostasis,[2] antioxidant defense,[1] therapeutic interventions,[1,3] and protective ability against diabete,[4] Alzheimer's and Parkinson's diseases.[5,6] CAR, ANS, and H-CAR are abundant in most vertebrates, while OPH seems to be rather more abundant in marine mammals and certain replies.[7] CAR and ANS are rich in meat products and have been used as an athlete supplement for many years.[8,9] With their potential physiological effects, these bioactive dipeptides are considered as bioactive food components. However, a main hurdle for utilizing such histidine-containing dipeptides as a food supplement is the low stability due to their rapid degradation by human serum carnosinase (CN) enzyme.[10−12] CN hydrolyzes histidine-containing dipeptides with different degrees of reactivity where CAR is the most favorable substrate.[13] Many strategies to extend a lifetime of such dipeptides, especially CAR, were studied.[14] A selective CN inhibitor, carnostatine (CARN) (SAN9812), was reported to effectively inhibit CN's activity.[14] A presence of H-CAR and ANS was found to retard CAR degradation.[11,15] Thus, the

Received: August 18, 2023
Revised: October 13, 2023
Accepted: October 19, 2023
Published: November 2, 2023

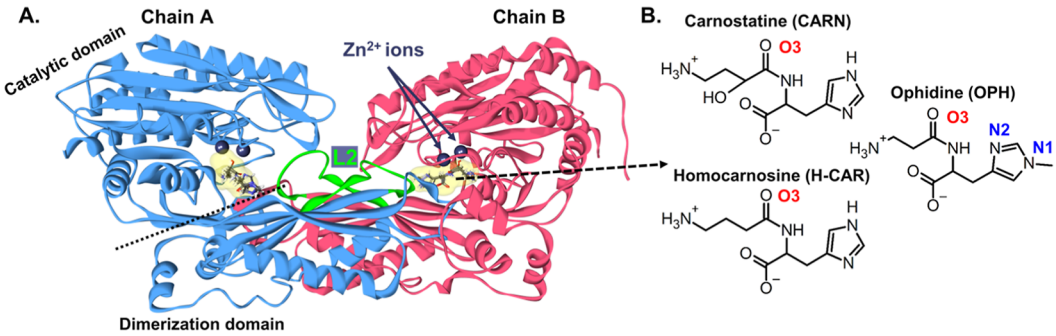

Figure 1. (A) Structure of the Zn^{2+}-containing CN1 homodimer. The catalytic and dimerization domains are displayed on chain A. The latching loops (L2) are labeled in green (residues 324−341). Chemical structures of CARN and H-CAR and OPH are shown in (B).

coadministration of natural analogues such as ANS was reported to significantly disrupt the CAR hydrolysis and eventually increase CAR level in blood plasma.[16] Recently, the binding mechanism of CAR and ANS to CN has been revealed,[17] whereas the binding of other substrates and inhibitor (CARN) remains obscure. The complete understanding of how CN recognizes and binds its substrates is crucial for designing an effective strategy to prolong the lifetime of CAR and its analogues after ingestion.

CNs are Xaa-His dipeptidases belonging to the metallopeptidase M20 family which cleaves histidine-containing dipeptides such as CAR and ANS to β-alanine and histidine.[13] CNs play diverse roles in protein maturation, tissue repair, and cell-cycle control.[18] A CN level was found to be correlated with diabetes and neurological disorders.[13,19,20] Two isoforms of CNs (Zn^{2+}-containing CN 1 (CN1) found in serum and Mn^{2+}-carnosinase 2 (CN2) in tissue) were identified with 49% sequence identity.[21,22] Both CNs exist as homodimers (chains A and B)[3] (Figure 1). Each chain consists of a catalytic domain and a dimerization domain (Figure 1A). The catalytic domain contains two Zn^{2+} ions at the active center (Figure 1A). Each chain has the latching loop (residues 324−341: L2) holding the two monomers together (a green loop in Figure 1A). Each monomer contains one zinc-centered binding pocket.[23] CN1 is the first and major hydrolyzer for histidine-containing dipeptides in serum, whereas the remaining is continuously degraded when they permeate into tissue.[24,25] Although CAR and ANS are major substrates, CN1 can also digest CAR analogues such as OPH and H-CAR[10,26] (Figure 1B). Research on OPH and H-CAR is less extensive because such chemicals do not mainly contribute to human diet.[27] The hydrolytic rate of CAR is the fastest followed by ANS, OPH, and H-CAR.[10,26] A presence of ANS was reported to reduce the hydrolysis of CAR.[11] As reported earlier, CAR and its analogues show physiological and therapeutic properties, but the short lifetime after ingestion due to their rapid degradation by CNs serves as a bottleneck for effective utilization. Therefore, an in-depth insight into the CN1 function is important for designing a potential strategy to extend a CAR lifetime. Although the binding mechanism of CAR, H-CAR, and ANS to CN1 has been reported recently,[17,28] the understanding of how CN1 recognizes and binds other substrates and especially inhibitor remains obscured. Thus, in this work, molecular dynamics (MD) simulations were employed to elucidate the binding mechanism of H-CAR, OPH, and CARN (CN inhibitor) in comparison to CAR and ANS binding from a previous work.[17]

MATERIALS AND METHODS

Preparation of Protein−Ligand Complexes. The crystal structure of the CN1 homodimer was downloaded from the RCSB protein databank (PDB ID: 3DLJ; resolution of 2.26 Å). Missing residues were modeled using Modeler 10.0.[29−31] Two Zn^{2+} ions were kept in each binding site. The protonation states of all charged residues were set at physiological pH. CARN, H-CAR, and OPH structures were built by Discovery studio visualizer.[31,32] All ligand topologies were generated using ACYPE with AMBER force field.[33] The partial atomic charge of ligands was calculated by the restrained electrostatic potential charge using the Hartree−Fock calculation with a 6-31G(d) basis set.[34] The AMBER99SB force field was used for the Zn^{2+} topology. All ligands were docked into the binding pocket of CN1 using GOLD5.3 software.[35,36] The default setting was used for docking. Residues within a distance of 10 Å from a ligand were defined as the binding site. No water is included in this docking step. For each ligand (H-CAR, OPH, and CARN), the CN1−ligand complex that has the highest gold-score was used for MD simulations (Table S1 and Figure S1 in Supporting Information). For MD setting, the CN1−ligand complex was placed in a cubic simulation box (dimension of 136 Å × 136 Å × 136 Å) and solvated with TIP3P water and counterions. 0.15 M NaCl was set for each system.

MD Simulations. GROMACS 2020 package (http://www.gromacs.org)[37] with AMBER99SB force field[38] was used for all MD simulations. To relax steric conflicts generated during setup, all energy minimizations of 1000 steps using the steepest descent algorithm were applied. Long-range electrostatic interactions were treated using the particle mesh Ewald method with a short-range cutoff of 1 nm, a Fourier spacing of 0.12 nm, and fourth-order spline interpolation. All simulations were performed in the constant number of particles, pressure, and temperature (*NPT*) ensemble. Protein, ligands, solvent and ions were coupled separately using the v-rescale thermostat[39] at 300 K with a coupling constant τ_t = 0.1 ps. The pressure was coupled using the Parrinello−Rahman barostat at 1 bar with a coupling constant τ_p = 1 ps. The time step for the integration was 2 fs. The 500 ps equilibration runs were performed in all systems and followed by the 500 ns production runs. Each system was repeated twice (the suffixes of "1 and "2" are used to represent simulation 1 and simulation 2). "CARN", "H-CAR", and "OPH" are used to represent ligand-bound CN1 complexes. The ending of "A" and "B" refer to chains A and B, respectively. In total, six simulations were performed (CARN1, CARN2, H-CAR1, H-CAR2, OPH1, and OPH2).

https://doi.org/10.1021/acsomega.3c06139
ACS Omega 2023, 8, 42966−42975

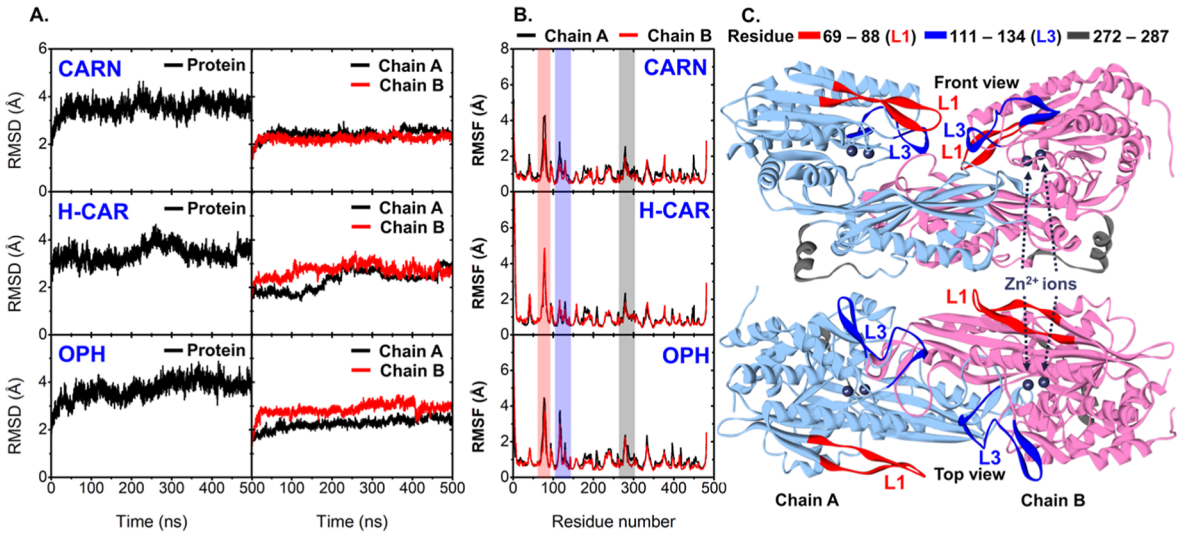

Figure 2. (A) C-α rmsds of the whole protein (left) and each chain (right). (B) C-α RMSFs of all systems where the highly fluctuated regions are shown as cartoon representatives in (C).

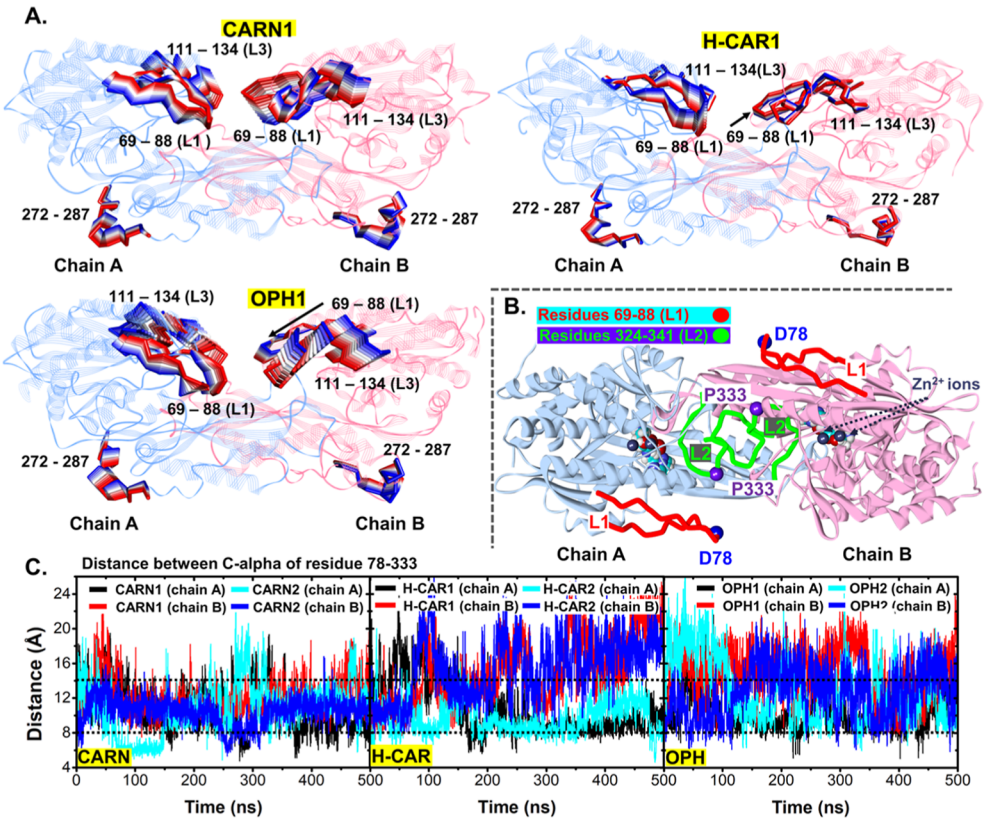

Figure 3. (A) PCA where only highly fluctuated regions are labeled. The dynamics was obtained from the first principal component (PC1) as a function of time, whose dynamics are represented in the RWB format. Only dominant motions are displayed for clear visualization. (B) Top view of CN1 labeled L1 and L2 where D78 and P333 at their tips are shown. (C) Distances between C-α atoms of D78 at the tip of L1 and P333 at the tip of L2 in all systems. L1 and L2 are labeled in red and green. The ligands are displayed in the vdW format.

All results provided here are the average values from two simulations. The data were analyzed by GROMACS and locally written code. Molecular graphic images were prepared using VMD.[40] C-α rmsd and RMSF calculations were computed using an initial structure at t = 0 ns as a reference. For principal component analysis (PCA), it was calculated by default "gmx covar" and "gmx anaeig" options in GROMACS. Only the first eigenvector was used to analyze the major protein motion in all cases. For hydrogen bond calculation, the hydrogen-donor−acceptor cutoff angle was 30°, and the cutoff radius (X-acceptor) of 0.35 nm was set. The Poisson−Boltzmann surface area (MM/PBSA) method was employed to calculate the binding free energy of association of the protein−ligand complex. MM/PBSA models were generated by using "gmx mmpbsa".

https://doi.org/10.1021/acsomega.3c06139
ACS Omega 2023, 8, 42966−42975

Table 1. Number of Hydrogen Bonds of Each Ligand with Water and Protein and the SASA in the Active Site

	number of hydrogen bonds					
	with water		with protein		SASA (nm^2)	
systems	chain A	chain B	chain A	chain B	chain A	chain B
CARN1	5.17 ± 1.74	2.47 ± 1.33	4.36 ± 1.87	8.93 ± 1.43	23.60 ± 0.71	21.57 ± 0.45
CARN2	5.92 ± 1.60	3.27 ± 1.50	3.76 ± 1.32	7.86 ± 1.76	23.71 ± 0.56	22.13 ± 0.51
H-CAR1	2.58 ± 1.29	2.00 ± 1.00	5.56 ± 1.48	5.13 ± 1.27	22.95 ± 0.49	22.32 ± 0.37
H-CAR2	3.76 ± 1.03	2.91 ± 1.17	3.67 ± 1.16	5.05 ± 1.26	20.93 ± 0.69	22.60 ± 0.48
OPH1	5.26 ± 1.39	2.56 ± 1.02	2.53 ± 0.98	4.22 ± 1.04	23.78 ± 0.52	22.29 ± 0.42
OPH2	5.08 ± 1.11	2.61 ± 1.15	2.53 ± 0.90	4.65 ± 1.19	23.79 ± 0.73	22.75 ± 0.50

Table 2. Interaction Energies (kJ/mol) with the Standard Deviation of All Ligands and Zn^{2+}-Bound CN1 in All Systems[a]

	chain A (kJ/mol)			chain B (kJ/mol)		
system	ΔE_{vdW}	ΔE_{Elec}	total energy	ΔE_{vdW}	ΔE_{Elec}	total energy
CARN1	−144.18 ± 15.82	−59.37 ± 27.23	−203.55 ± 27.97	−100.50 ± 20.54	−504.87 ± 27.13	−605.37 ± 24.29
CARN2	−138.94 ± 10.76	−107.04 ± 23.82	−245.98 ± 24.60	−108.87 ± 22.07	−495.08 ± 27.87	−603.95 ± 23.78
H-CAR1	−133.38 ± 10.57	−122.91 ± 19.31	−256.29 ± 21.23	−137.12 ± 13.51	−203.69 ± 16.29	−340.82 ± 13.69
H-CAR2	−149.65 ± 12.92	−140.66 ± 13.17	−290.32 ± 14.85	−119.34 ± 16.15	−192.31 ± 19.98	−311.65 ± 21.58
OPH1	−137.17 ± 9.40	−86.59 ± 19.65	−223.75 ± 20.15	−127.27 ± 13.29	−185.65 ± 12.88	−312.92 ± 13.50
OPH2	−157.06 ± 8.97	−109.37 ± 13.44	−266.43 ± 15.72	−129.87 ± 14.05	−189.87 ± 14.72	−319.74 ± 13.58

[a]The data after 350 ns were used to calculate the interaction energies.

RESULTS AND DISCUSSION

The structural drift and fluctuation of ligand-bound CN1 complexes were measured using C-α root-mean-square deviations (rmsds) and fluctuations (RMSFs) (Figure 2). The initial structure at time = 0 ns was employed as a reference for rmsd and RMSF calculations. Comparing to CAR- and ANS-bound CN1 complexes from a previous work,[17] the binding of CARN seems to promote similar structural flexibility to the binding of CAR and ANS, whereas H-CAR and especially OPH induce slightly higher structural mobility (Figure 2A). The binding of H-CAR and OPH also causes different structural flexibilities between each monomer (Figure 2A; right). This difference is also seen in the ANS−CN1 complex.[17] Especially, chain B of H-CAR and OPH clearly displays a higher flexibility than chain A, while a nearly identical degree of structural mobility is observed between monomers in CARN. Apparently, bound CAR and CARN promote a low structural drift, while the binding of H-CAR and OPH enhances the protein flexibility. It is noticeable in Figure 2B,C that the origin of protein fluctuation is from the mobility of residues 69−88 (L1), 111−134 (L3), and 272−287, respectively. Especially, the β-hairpin L1 loop (a red region in Figure 2B,C) shows the most prominent fluctuation. For the OPH, the structural fluctuation of L3 is also captured (blue regions in Figure 2C). Not only L1 and L3, a short helical region (residues 272−287) is also slightly flexible. These dynamic events were also observed in previous work.[17,22,28]

PCA can also confirm the high fluctuation of residues L1, L3, and 272−287 (Figure 3A). Only the first principal component was used in this calculation because it accounts for the main motion (Figure S2 in Supporting Information). All PCAs can be seen in Figure S3 in Supporting Information. Among all of them, the L1 loops in all systems seem to show the highest fluctuation, especially the OPH (Figure 3A). The β-hairpin L1 region was reported to be involved in the gating activity;[22] thus, its motion may affect the ability to accommodate a ligand. To further explore the dynamics of L1, the distances between the tip of L1 (D78) and L2 (P333) were measured (Figure 3B,C). It can be seen that the high fluctuations of the L1−L2 distances are captured in H-CAR and the OPH, while the binding of CARN causes less loop mobility (Figure 3B,C). Even though some fluctuation is observed, the dynamics of L1 in all monomers of CARN appears to be similar. L1−L2 distances in both monomers of CARN seem to be fluctuated in the range of ∼8−14 Å (Figure 3B) where L1 is shifted toward L2 region (Figure 3A). In contrast, the L1−L2 distances in both the OPH and H-CAR are different from those of the CARN (Figure 3A). L1 in OPH and H-CAR seems to swing away from the center, resulting in the elongation of L1−L2 distances (Figure 3C). Additionally, the dissimilar degrees of L1 mobility in each subunit of OPH and H-CAR are captured. In H-CAR, chain B appears to produce the large L1 movement, while chain A displays a more rigid L1 (Figure 3C). On the contrary, the high mobility of L1 in both OPH1 and OPH2 is found. This large L1 drift can thus explain the high structural flexibility of the OPH, as seen in Figure 2A. A monomer with L1 packed close to the active site should be more ready to conduct a catalysis than a monomer with the gating L1 staying away from the pocket. The diverse L1 motion does not only reflect the different gating activities between monomers but also confirms the nonsynchronized function between subunits, as seen in previous studies.[17] Interestingly, the presence of the CARN inhibitor seems to tether L1 to the protein core. L1 in CARN is likely to move toward the active site and shows less mobility (Figure 3A,C). This phenomenon is also preserved in both monomers. The basic finding here can also demonstrate that CARN binding enhances protein rigidity.

Considering the interactions of each ligand with its environment, the binding of OPH seems to be looser to CN1, while CARN displays the firm binding, especially in chain B (Table 1). Based on the interactions with a protein, CARN seems to be the most favorable for CN1, followed by H-CAR, and OPH, respectively (Table 1). Besides, a high number of interactions with CN1 induces the lowering of

https://doi.org/10.1021/acsomega.3c06139
ACS Omega 2023, 8, 42966−42975

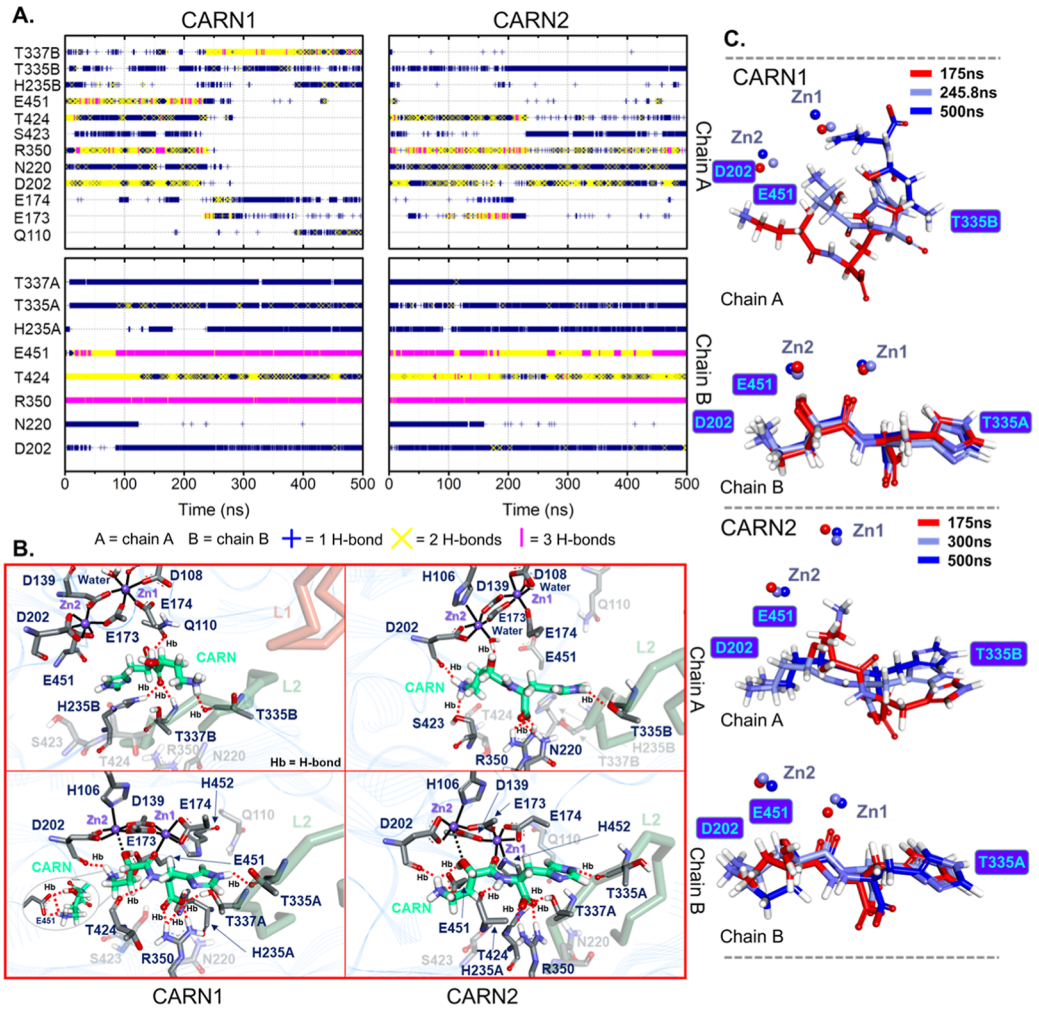

Figure 4. (A) Number of hydrogen bonds between CN1 and CARN in all systems. The locations of key components are displayed in (B). (C) Conformational changes of CARN1 and CARN2 and zinc ions as functions of time.

water interactions. The additional hydroxyl group in CARN allows it to form more hydrogen bonds than others (~7−9 hydrogen bonds in Table 1), resulting in fewer water contacts (~2−3 water contacts in Table 1). Unlike CARN, the smallest ligand (OPH) is trapped inside CN1 by ~3−5 hydrogen bonds. It is noticeable that chain B induces a better fit for ligand than chain A due to higher protein−ligand interactions (Table 1). This finding highlights that CN1 monomers work independently. Inside a pocket, a presence of various ligand still provides a comparable degree of solvent-accessible surface areas (SASA) (Table 1). CN1 appears to have a SASA of ~21−24 nm^2. The better grip for a ligand in chain B can shrink the binding pocket down to ~21−22 nm^2, while chain A with more water exposure induces a slightly larger pocket (~23 nm^2) (Table 1). However, only H-CAR2 shows the larger pocket in chain A than chain B. This ligand produces a comparable number of protein−ligand and water−ligand hydrogen bonds (~4 interactions; Table 1). Comparing with H-CAR and OPH, CN1 provides the best fit for CARN. With the ability to tightly bind CN1, CARN can act as a good CN1 inhibitor.

To further investigate the binding affinities of ligands, the interaction energies are also computed via MMPBSA[41] (Table 2). It can be confirmed in Table 2 that chain B provides a better environment for ligand binding in all cases. All ligands seem to bind chain A with a similar degree of binding affinities (interaction energies of ~−310 to −340 kJ/mol), whereas chain B clearly prefers CARN to others (interaction energy of ~−600 kJ/mol) where H-CAR and OPH show similar binding affinities (Table 2). Chain A seems to show non selectivity for all ligands using both electrostatic and hydrophobic interactions, while the high selectivity for CARN is captured in chain B using electrostatic forces (Table 2). Comparing with ANS and CAR which are main CN1 substrates (interaction energies of ~285−319 kJ/mol),[17] CARN clearly displays the highest binding affinities (interaction energy of ~600 kJ/mol). This finding not only confirms the tighter binding of CARN than the main substrates but also reflects the effective competitive inhibition ability of CARN against CN1.

In Figures 4−6, the further hydrogen bonds between each ligand and the key residues are computed. The results agree well with the total protein−ligand hydrogen bonds in Table 1 that CARN forms the highest number of protein−ligand interactions due to its ability to interact with multiple pocket-lining residues. Moreover, the different degrees of rigidity of the bound ligand in each subunit confirm the dissimilar capability of each monomer to accommodate ligand (Figure 4C). This finding is in a good agreement with previous studies.[17] Comparing with chain A, chain B induces less ligand mobility, suggesting tighter ligand binding, while the ligand

https://doi.org/10.1021/acsomega.3c06139
ACS Omega 2023, 8, 42966−42975

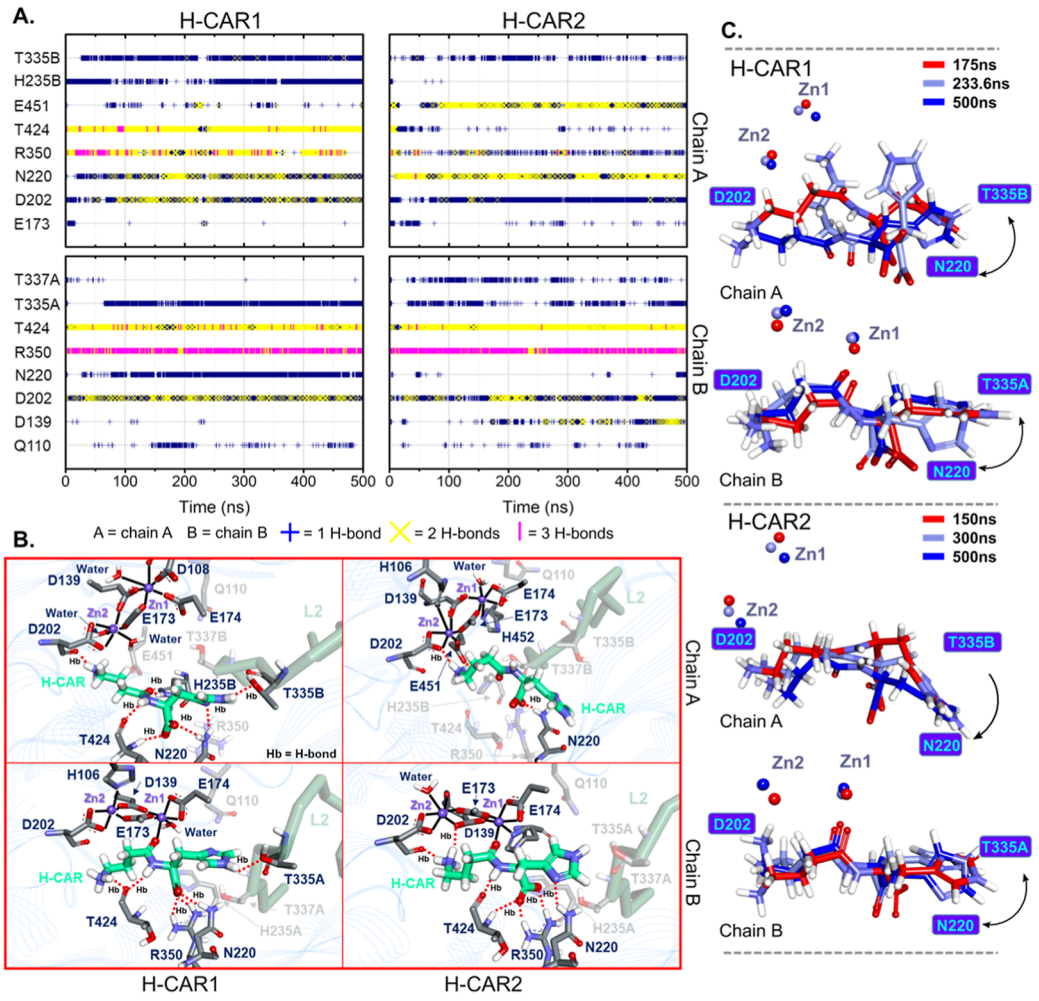

Figure 5. (A) Number of hydrogen bonds between CN1 and H-CAR in all systems. The locations of key components are displayed in (B). (C) Conformational changes of H-CAR1 and H-CAR2 and zinc ions in all chains as a function of time.

displacement is captured in chain A, especially CARN1 (Figures 4C, 5C, and 6C). For CARN inhibitors, both simulations (CARN1 and CARN2) clearly show the tight ligand binding in chain B, whereas CARN in chain A is mobile, resulting in the reorientation (Figure 4). CARN in chain B is trapped by strong and permanent interactions with D202, R350, T424, and E451 and H235A, T335A, and T337A (the ending "A" refers to "from chain A") (Figure 4A,B). An amine ($-NH_3$) end of CARN is anchored by D202 and E451, whereas its imidazole moiety pointing toward the opposite site is stabilized by T335A (Figure S4 in Supporting Information). At the mid of the backbone, the amide nitrogen interacts with T424, whereas the carboxylic group is tethered by R350, and H235A and T337A from an adjacent unit, which also suggests the importance of being dimer for CN1 function (Figures 1B, 4, and S4). Also, the additional hydroxyl group of CARN appears to interact with E451. The amide oxygen (O3) also points toward the Zn site. On the contrary, chain A promotes the loose ligand binding, resulting in the displacement of both CARN1 and CARN2 (Figure 4C). Apparently, in CARN1, ligand relocation in chain A is initiated by the loss of CN1-CARN interactions at the amine terminus. It seems to lose its main interaction with E451, resulting in the flip of CARN in CARN1 and the twisting of the $-NH_3$ group in CARN2 (Figure S4B in Supporting Information). For CARN1, the flip of CARN1A allows the formation of a new interaction network with Q110, E173, and E174 (Figure 4). For CARN2, although no serious drift of ligand orientation is captured, the breakdown of NH3-E451interactions triggers the twisting of the $-NH_3$ end leading to the destabilized CARN2A structure (Figure 4C). Moreover, the escape of O3 on CARN in chain A facilitates the shift of CARN away from the zinc site, as seen in Figure 4C.

For H-CAR which shares a similar structure with CARN, H-CAR thus employs a similar interaction network to CARN. H-CAR in chain A shows high structural fluctuation as similar as CARN (Figures 4C and 5C). For flexible H-CAR in chain A, the $-NH_3$ end is mainly trapped by D202 where H-CAR has an additional interaction with T424 in H-CAR1 and E451 in H-CAR2 (Figure S5 in Supporting Information). However, an imidazole ring remains anchored inside by hydrogen bonds with N220 and T335B from the adjacent subunit (Figures 5 and S5). H-CAR also employs its carboxyl group ($-COO^-$) to form strong hydrogen bonds with N220 and R350 (Figures 5 and S5). Comparing to CARN, the absence of the hydroxyl group ($-OH$) seems to enhance the flexibility of $-NH_3$ end. This high mobility appears to significantly increase the flexibility of the entire H-CAR structure (Figure 5C). For H-CAR in chain B, the tight binding of the ligand is due to the strong and permanent interactions with D202, T424, R350,

https://doi.org/10.1021/acsomega.3c06139
ACS Omega 2023, 8, 42966−42975

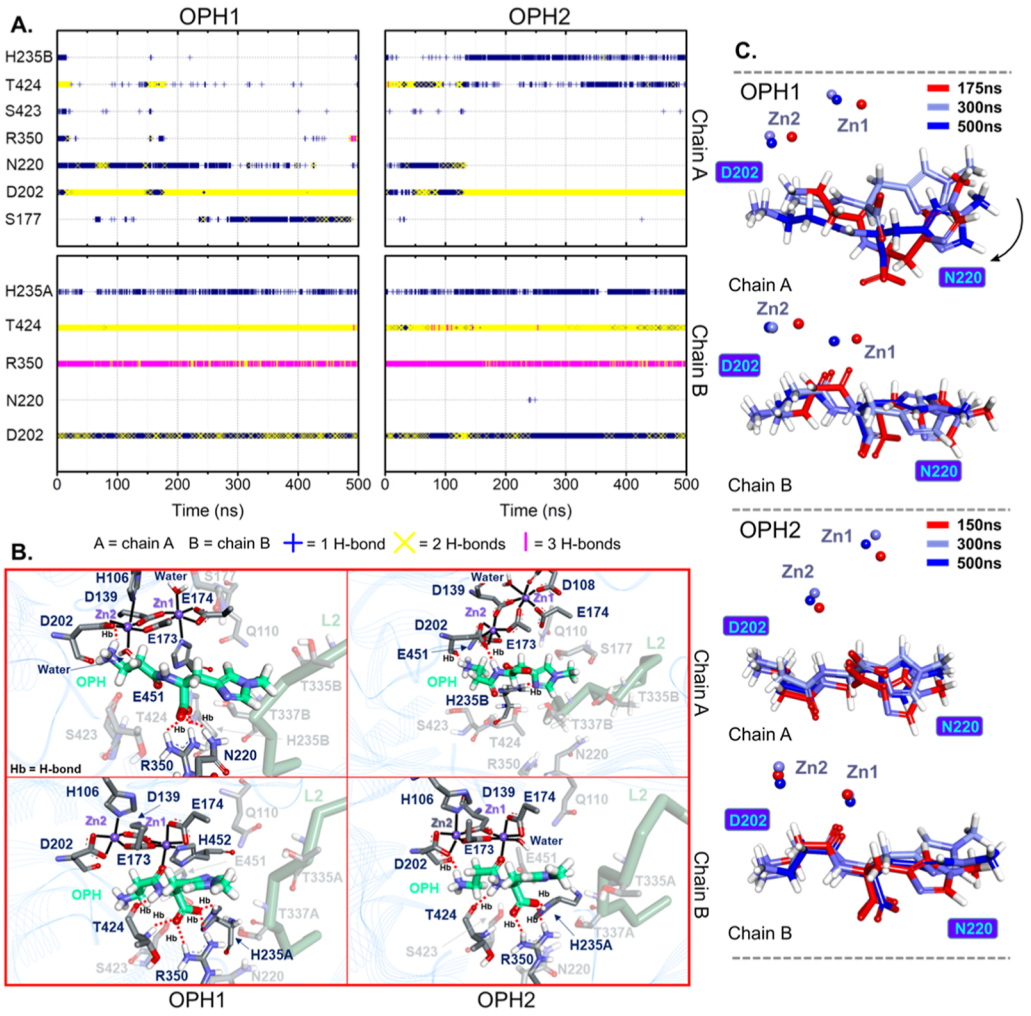

Figure 6. (A) Number of hydrogen bonds between CN1 and the OPH in all systems. The locations of key components are displayed in (B). (C) Conformational changes of OPH1 and OPH2 and zinc ions in all chains as a function of time.

and T335A from an adjacent monomer, whereas the additional interaction with T337A is captured in H-CAR2 (Figure 5). Similar to CARN, the amide oxygen (O3) in chain A is shifted away from the Zn site in all cases. This highlights the nonspontaneous catalytic activities between monomers (Figure S6 in Supporting Information) where chain B displays the better ligand-binding ability.

In case of OPH, a small number of CN1-OPH hydrogen bonds in Figure 6 indicates the low binding affinity of OPH to CN1 which agrees well with previous experimental studies.[10,26] Only OPH1A shows high flexibility, whereas only slightly mobile OPHs are observed in other systems (Figure 6B,C). Nonetheless, chain A seems to be not suitable for OPH hydrolysis since the displacement of both Zn^{2+} ions is captured (Figure 6C). OPH contains the shortest amine chain and a methylimidazole ring, but its $-NH_3$ end can interact with D202, while its backbone forms hydrogen bonds with R350, T424, and H235 from an adjacent unit (Figures 6C and S7 in Supporting Information). Seemingly, the low catalytic activity of OPH reported experimentally can be due to the absence of interaction between CN1 and a methylimidazole ring (Figures 6 and S7 in Supporting Information). This finding can also explain why OPH shows the low binding affinity consequently leading to the lowest hydrolytic rate observed in a previous work.[10,26]

In many dizinc aminopeptidases, the hydrolysis is propagated by the attack of either zinc-mediating water molecules or hydroxide ion.[42,43] For water-mediating system, both zinc ions (Zn1 and Zn2) were reported to be dynamically bridged by D139 and E173 where Zn^{2+} ions have more water exposure in chain A.[17,22] In case of hydroxide-mediating reaction, an earlier study reported the Zn-D139 interaction, where no Zn-E173 interaction was suggested due to the protonation of E173.[28] Herein, only the condition of water mediation is investigated due to its abundance. Zn1 and Zn2 are found to be coordinated by D139 and E173 as seen in previous work.[17,22] Not only the bridging D139 and E173 but also each zinc ion interacts with ∼1−2 surrounding amino acids or water molecules (Figure 7). D108 and E174 interact with Zn1 in chain A, while only E174 contributes to trapping Zn1 in chain B (Figure 7). For Zn2, chain A employs D202 and E451 to stabilize Zn2, while only D202 is required to keep Zn2 in chain B (Figure 7). Also, the more water-exposed Zn^{2+} ions in chain A allow the displacement of both Zn^{2+} ions (Figures 4C, 5C, 6C, and S6 in Supporting Information). For chain A, the shift of the active carbonyl oxygen (O3) away from Zn1 is captured. Such shift causes the flip of O3 toward H235B which can be confirmed by close O3-H235B distances (Figure S6 in Supporting Information). These findings indicate the functional unreadiness of chain A. Unlike chain A, the

https://doi.org/10.1021/acsomega.3c06139
ACS Omega 2023, 8, 42966−42975

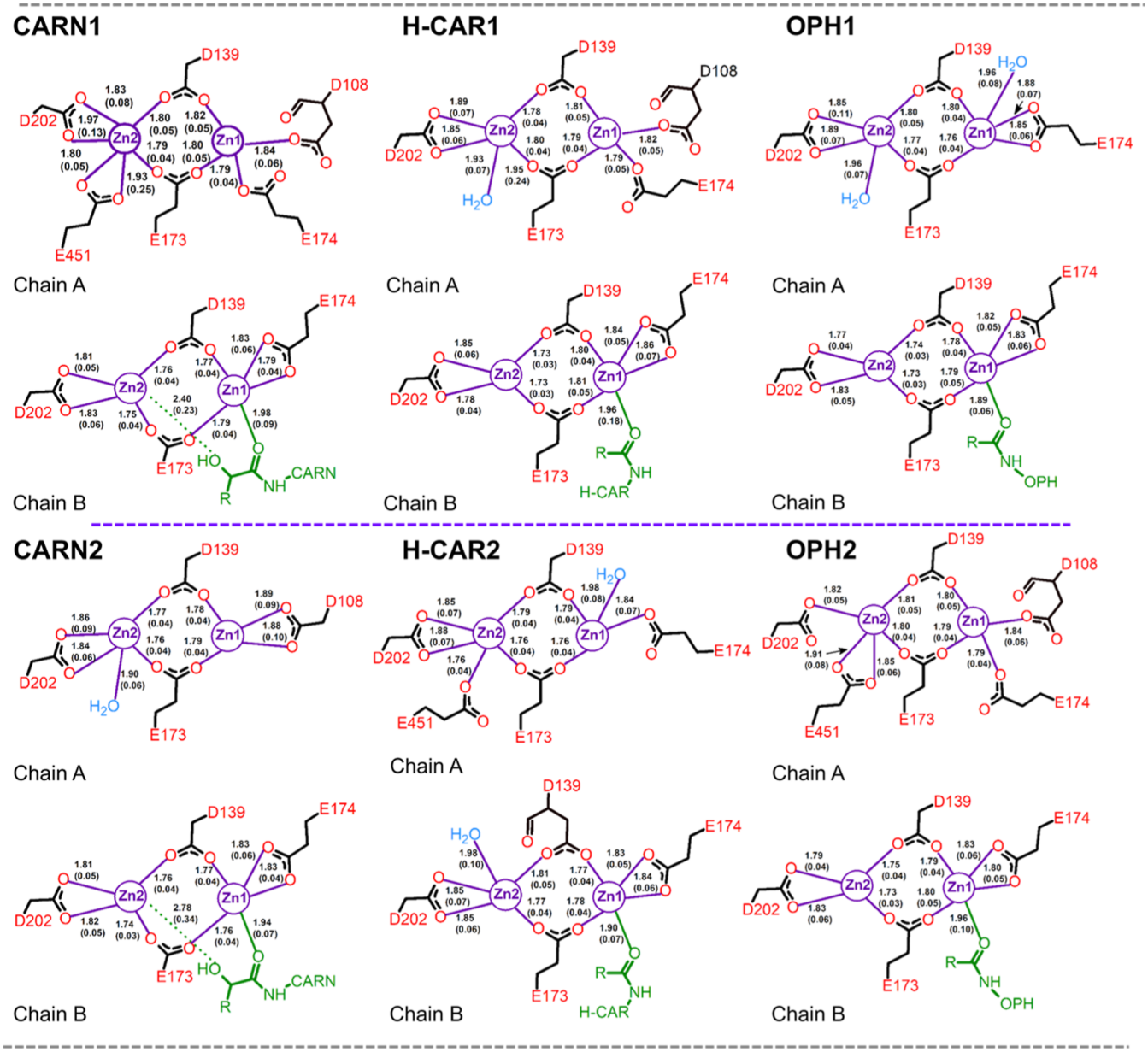

Figure 7. Environment of all Zn^{2+} ions (Zn1 and Zn2) in all systems.

dehydrated pocket of chain B allows zinc ions to pair with a ligand (Figures 7 and S8), resulting in firm ligand binding. The active carbonyl oxygen (O3) of ligand points toward the Zn site in chain B (Zn−O3 distance of ∼2 Å in Figure S6, which is in a range of Zn−O bond length reported in previous metalloprotein studies[44−46]). No contact of the O3-H235B is identified in chain B (Figure S6). The oxygen O3 in chain B directly points toward the Zn site. This scenario can facilitate the catalysis. The different ligand-binding environments provided by each monomer confirm the independent and nonsimultaneous function of each subunit as seen in previous studies.[17]

CONCLUSIONS

In this work, the binding mechanism of H-CAR and OPH, which are natural CN1 substrates, and the CARN inhibitor to CN1 is investigated. Herein, it is evident that CN1 monomers work independently and nonsimultaneously. Also, being a dimer is required for CN1 to function. Among all possible substrates,[17] CARN shows the highest binding affinity to CN1, indicating the robust inhibitory effects of CARN which agrees well with a previous experimental work.[14] However, no molecular information about the root of such effective inhibition has been reported. Overall, the amine end and imidazole ring are the main players in trapping all ligands in a pocket. The degree of the ligand-binding ability seems to be influenced by the interactions of both moieties. Herein, although CARN has the longer amine end (one additional −CH_2− chain) than CAR (the most favorable substrate), the additional hydroxyl group (−OH) on CARN can strengthen its binding affinity by strongly interacting with E451. This trap also promotes the tighter binding of CARN. The key role of −OH can be comparatively confirmed by the binding mechanism of H-CAR (a CARN analogue) where the absence of −OH causes the mobile amine end, resulting in the reduction of CN1-H-CAR interactions as reported earlier in

https://doi.org/10.1021/acsomega.3c06139
ACS Omega 2023, 8, 42966−42975

the text. For OPH which is an analogue of ANS (one of the favorable substrates) where a methyl ($-CH_3$) group is attached on N1 of an imidazole ring (Figure 1C), this methyl group eliminates the imidazole ring-CN1 interaction network, resulting in the loose ligand binding ability of OPH.

In summary, this work provides a molecular explanation of how substrates (H-CAR and OPH) and inhibitor (CARN) bind to CN1. Comparing with preferred substrate (CAR), the structural rigidity and proper pose seem to be the key to determine the binding affinity and sequentially the hydrolytic capability. CARN binds tighter to CN1 due to its extra interactions between −OH and CN1, whereas H-CAR and OPH bind looser to CN1 because of the lack of CN1−ligand interactions. Our results agree with a previous computational work that H-CAR shows lightly higher number of interactions with CN1 than CAR (the most favorable substrate),[28] but poor hydrolysis of H-CAR is identified here due to the shift of active oxygen (O3) away from the zinc site. So does OPH. Comparing to the binding poses of CAR and ANS from previous studies,[17] O3 of H-CAR and OPH are slightly further away from Zn1 which can be one of the roots for poorer catalytic activity.

■ ASSOCIATED CONTENT

Data Availability Statement

The data that support the findings of this study are available from https://drive.google.com/drive/folders/1p1OE3pQK2BRK87awAfO2mp8ie7-AD72G?usp=sharing.

Supporting Information

The Supporting Information is available free of charge at https://pubs.acs.org/doi/10.1021/acsomega.3c06139.

Binding modes; eigenvalues; PCA; number of hydrogen bonds of CARN, H-CAR, and OPH; distances of Zn ions; and hydrogen bonds between ligand and water (PDF)

■ AUTHOR INFORMATION

Corresponding Author

Prapasiri Pongprayoon − *Department of Chemistry, Faculty of Science, Kasetsart University, Bangkok 10900, Thailand; Center for Advanced Studies in Nanotechnology for Chemical, Food and Agricultural Industries, KU Institute for Advanced Studies, Kasetsart University, Bangkok 10900, Thailand;* orcid.org/0000-0002-1472-8241; Phone: +66-2562-5555; Email: fsciprpo@ku.ac.th; Fax: +66-2579-3955

Authors

Borvornwat Toviwek − *Department of Chemistry, Faculty of Science, Kasetsart University, Bangkok 10900, Thailand*

Thanathip Suwanasopee − *Department of Animal Science, Faculty of Agriculture, Kasetsart University, Bangkok 10900, Thailand*

Skorn Koonawootrittriron − *Department of Animal Science, Faculty of Agriculture, Kasetsart University, Bangkok 10900, Thailand*

Danai Jattawa − *Department of Animal Science, Faculty of Agriculture, Kasetsart University, Bangkok 10900, Thailand*

Complete contact information is available at: https://pubs.acs.org/10.1021/acsomega.3c06139

Notes

The authors declare no competing financial interest.

■ ACKNOWLEDGMENTS

We would like to thank the Kasetsart University Research and Development Institute (KURDI) (grant no. FF(KU) 7.66) and the Office of the National Economic and Social Development Council, the Office of the Prime Minister through Kasetsart University under the project entitled "Driving Research and Development of Cutting-edge Innovations for ASEAN's Agricultural Leadership" for financial support. We are also thankful for the computer facilities from Department of Computer Engineering, Kasetsart University and NSTDA Supercomputer Center (ThaiSC).

■ ABBREVIATIONS

MD, molecular dynamics
CN1, carnosinase 1
CAR, carnosine
ANS, anserine
CARN, carnostatine
H-CAR, homocarnosine
OPH, ophidine

■ REFERENCES

(1) Derave, W.; De Courten, B.; Baba, S. P. An update on carnosine and anserine research. *Amino Acids* **2019**, *51* (1), 1−4.

(2) Blancquaert, L.; Baba, S. P.; Kwiatkowski, S.; Stautemas, J.; Stegen, S.; Barbaresi, S.; Chung, W.; Boakye, A. A.; Hoetker, J. D.; Bhatnagar, A.; et al. Carnosine and anserine homeostasis in skeletal muscle and heart is controlled by β-alanine transamination. *J. Physiol.* **2016**, *594* (17), 4849−4863.

(3) Boldyrev, A. A.; Aldini, G.; Derave, W. Physiology and pathophysiology of carnosine. *Physiol. Rev.* **2013**, *93* (4), 1803−1845.

(4) Pavlin, M.; Rossetti, G.; De Vivo, M.; Carloni, P. Carnosine and Homocarnosine Degradation Mechanisms by the Human Carnosinase Enzyme CN1: Insights from Multiscale Simulations. *Biochemistry* **2016**, *55* (19), 2772−2784.

(5) Davies, K. M.; Bohic, S.; Carmona, A.; Ortega, R.; Cottam, V.; Hare, D. J.; Finberg, J. P.; Reyes, S.; Halliday, G. M.; Mercer, J. F.; et al. Copper pathology in vulnerable brain regions in Parkinson's disease. *Neurobiol. Aging* **2014**, *35* (4), 858−866.

(6) Hipkiss, A. R. Carnosine, diabetes and Alzheimer's disease. *Expert Rev. Neurother.* **2009**, *9* (5), 583−585.

(7) Kwiatkowski, S.; Kiersztan, A.; Drozak, J. Biosynthesis of Carnosine and Related Dipeptides in Vertebrates. *Curr. Protein Pept. Sci.* **2018**, *19* (8), 771−789.

(8) Oppermann, H.; Elsel, S.; Birkemeyer, C.; Meixensberger, J.; Gaunitz, F. Erythrocytes Prevent Degradation of Carnosine by Human Serum Carnosinase. *Int. J. Mol. Sci.* **2021**, *22* (23), 12802.

(9) Saunders, B.; Elliott-Sale, K.; Artioli, G. G.; Swinton, P. A.; Dolan, E.; Roschel, H.; Sale, C.; Gualano, B. β-alanine supplementation to improve exercise capacity and performance: a systematic review and meta-analysis. *Br. J. Sports Med.* **2017**, *51* (8), 658−669.

(10) Gilardoni, E.; Gervasoni, S.; Maspero, M.; Dallanoce, C.; Vistoli, G.; Carini, M.; Aldini, G.; Regazzoni, L. Development of a direct LC-ESI-MS method for the measurement of human serum carnosinase activity. *J. Pharm. Biomed. Anal.* **2020**, *189*, 113440.

(11) Peters, V.; Jansen, E. E.; Jakobs, C.; Riedl, E.; Janssen, B.; Yard, B. A.; Wedel, J.; Hoffmann, G. F.; Zschocke, J.; Gotthardt, D.; et al. Anserine inhibits carnosine degradation but in human serum carnosinase (CN1) is not correlated with histidine dipeptide concentration. *Clin. Chim. Acta* **2011**, *412* (3−4), 263−267.

(12) Aldini, G.; Orioli, M.; Rossoni, G.; Savi, F.; Braidotti, P.; Vistoli, G.; Yeum, K.-J.; Negrisoli, G.; Carini, M. The carbonyl scavenger carnosine ameliorates dyslipidaemia and renal function in Zucker obese rats. *J. Cell. Mol. Med.* **2011**, *15* (6), 1339−1354.

(13) Bellia, F.; Vecchio, G.; Rizzarelli, E. Carnosinases, their substrates and diseases. *Molecules* **2014**, *19* (2), 2299−2329.

(14) Qiu, J.; Hauske, S. J.; Zhang, S.; Rodriguez-Niño, A.; Albrecht, T.; Pastene, D. O.; van den Born, J.; van Goor, H.; Ruf, S.; Kohlmann, M.; et al. Identification and characterisation of carnostatine (SAN9812), a potent and selective carnosinase (CN1) inhibitor with in vivo activity. *Amino Acids* **2019**, *51* (1), 7−16.
(15) Peters, V.; Kebbewar, M.; Jansen, E. W.; Jakobs, C.; Riedl, E.; Koeppel, H.; Frey, D.; Adelmann, K.; Klingbeil, K.; Mack, M.; et al. Relevance of allosteric conformations and homocarnosine concentration on carnosinase activity. *Amino Acids* **2010**, *38* (5), 1607−1615.
(16) Everaert, I.; Taes, Y.; De Heer, E.; Baelde, H.; Zutinic, A.; Yard, B.; Sauerhofer, S.; Vanhee, L.; Delanghe, J.; Aldini, G.; et al. Low plasma carnosinase activity promotes carnosinemia after carnosine ingestion in humans. *Am. J. Physiol.: Renal Physiol.* **2012**, *302* (12), F1537−F1544.
(17) Toviwek, B.; Koonawootrittriron, S.; Suwanasopee, T.; Pongprayoon, P. Molecular insights into the binding of carnosine and anserine to human serum carnosinase 1 (CN1). *PeerJ Phys. Chem.* **2022**, *4*, No. e25.
(18) Chen, S.-L.; Marino, T.; Fang, W.-H.; Russo, N.; Himo, F. Peptide Hydrolysis by the Binuclear Zinc Enzyme Aminopeptidase from Aeromonas proteolytica: A Density Functional Theory Study. *J. Phys. Chem. B* **2008**, *112* (8), 2494−2500.
(19) Peters, V.; Zschocke, J.; Schmitt, C. P. Carnosinase, diabetes mellitus and the potential relevance of carnosinase deficiency. *J. Inherit. Metab. Dis.* **2018**, *41* (1), 39−47.
(20) Janssen, B.; Hohenadel, D.; Brinkkoetter, P.; Peters, V.; Rind, N.; Fischer, C.; Rychlik, I.; Cerna, M.; Romzova, M.; de Heer, E.; et al. Carnosine as a protective factor in diabetic nephropathy: association with a leucine repeat of the carnosinase gene CNDP1. *Diabetes* **2005**, *54* (8), 2320−2327.
(21) Teufel, M.; Saudek, V.; Ledig, J. P.; Bernhardt, A.; Boularand, S.; Carreau, A.; Cairns, N. J.; Carter, C.; Cowley, D. J.; Duverger, D.; et al. Sequence identification and characterization of human carnosinase and a closely related non-specific dipeptidase. *J. Biol. Chem.* **2003**, *278* (8), 6521−6531.
(22) Tancharoen, C.; Tovivek, B.; Niramitranon, J.; Kityakarn, S.; Luksirikul, P.; Gorinstein, S.; Pongprayoon, P. Exploring the structural and dynamic differences between human carnosinase I (CN1) and II (CN2). *Proteins: Struct., Funct., Bioinf.* **2023**, *91*, 822−830.
(23) Unno, H.; Yamashita, T.; Ujita, S.; Okumura, N.; Otani, H.; Okumura, A.; Nagai, K.; Kusunoki, M. Structural basis for substrate recognition and hydrolysis by mouse carnosinase CN2. *J. Biol. Chem.* **2008**, *283* (40), 27289−27299.
(24) Boldyrev, A. A.; Aldini, G.; Derave, W. Physiology and Pathophysiology of Carnosine. *Physiol. Rev.* **2013**, *93* (4), 1803−1845.
(25) Baguet, A.; Everaert, I.; Yard, B.; Peters, V.; Zschocke, J.; Zutinic, A.; De Heer, E.; Podgórski, T.; Domaszewska, K.; Derave, W. Does low serum carnosinase activity favor high-intensity exercise capacity? *J. Appl. Physiol.* **2014**, *116* (5), 553−559.
(26) Pegova, A.; Abe, H.; Boldyrev, A. Hydrolysis of carnosine and related compounds by mammalian carnosinases. *Comp. Biochem. Physiol., Part B: Biochem. Mol. Biol.* **2000**, *127* (4), 443−446.
(27) de Jager, S.; Vermeulen, A.; De Baere, S.; Van der Stede, T.; Lievens, E.; Croubels, S.; Jäger, R.; Purpura, M.; Bourgois, J. G.; Derave, W. Acute balenine supplementation in humans as a natural carnosinase-resistant alternative to carnosine. *Sci. Rep.* **2023**, *13* (1), 6484.
(28) Pavlin, M.; Rossetti, G.; De Vivo, M.; Carloni, P. Carnosine and Homocarnosine Degradation Mechanisms by the Human Carnosinase Enzyme CN1: Insights from Multiscale Simulations. *Biochemistry* **2016**, *55* (19), 2772−2784.
(29) Martí-Renom, M. A.; Stuart, A. C.; Fiser, A.; Sánchez, R.; Melo, F.; Sali, A. Comparative protein structure modeling of genes and genomes. *Annu. Rev. Biophys. Biomol. Struct.* **2000**, *29*, 291−325.
(30) Šali, A.; Blundell, T. L. Comparative Protein Modelling by Satisfaction of Spatial Restraints. *J. Mol. Biol.* **1993**, *234* (3), 779−815.
(31) Webb, B.; Sali, A. Comparative Protein Structure Modeling Using MODELLER. *Curr. Protoc. Bioinf.* **2016**, *54* (1), 5.6.1−5.6.37.
(32) BIOVIA, Dassault Systèmes. *Discovery Studio Visualizer, v21.1.020298*; Dassault Systèmes: San Diego, 2021.
(33) Sousa da Silva, A. W.; Vranken, W. F. ACPYPE - AnteChamber PYthon Parser interfacE. *BMC Res. Notes* **2012**, *5* (1), 367.
(34) Bayly, C. I.; Cieplak, P.; Cornell, W.; Kollman, P. A. A well-behaved electrostatic potential based method using charge restraints for deriving atomic charges: the RESP model. *J. Phys. Chem.* **1993**, *97* (40), 10269−10280.
(35) Jones, G.; Willett, P.; Glen, R. C.; Leach, A. R.; Taylor, R. Development and validation of a genetic algorithm for flexible docking 1 1Edited by F. E. Cohen. *J. Mol. Biol.* **1997**, *267* (3), 727−748.
(36) Verdonk, M. L.; Cole, J. C.; Hartshorn, M. J.; Murray, C. W.; Taylor, R. D. Improved protein-ligand docking using GOLD. *Proteins* **2003**, *52* (4), 609−623.
(37) Lindahl, E.; Hess, B.; van der Spoel, D. GROMACS 3.0: a package for molecular simulation and trajectory analysis. *J. Mol. Model.* **2001**, *7* (8), 306−317.
(38) Hornak, V.; Abel, R.; Okur, A.; Strockbine, B.; Roitberg, A.; Simmerling, C. Comparison of multiple Amber force fields and development of improved protein backbone parameters. *Proteins* **2006**, *65* (3), 712−725.
(39) Bussi, G.; Donadio, D.; Parrinello, M. Canonical sampling through velocity rescaling. *J. Phys. Chem. A* **2007**, *126* (1), 014101.
(40) Humphrey, W.; Dalke, A.; Schulten, K. VMD: Visual molecular dynamics. *J. Mol. Graph.* **1996**, *14* (1), 33−38.
(41) Kumari, R.; Kumar, R.; Lynn, A. g_mmpbsa—A GROMACS Tool for High-Throughput MM-PBSA Calculations. *J. Chem. Inf. Model.* **2014**, *54* (7), 1951−1962.
(42) Lindner, H. A.; Lunin, V. V.; Alary, A.; Hecker, R.; Cygler, M.; Menard, R. Essential roles of zinc ligation and enzyme dimerization for catalysis in the aminoacylase-1/M20 family. *J. Biol. Chem.* **2003**, *278* (45), 44496−44504.
(43) Straeter, N.; Lipscomb, W. N. Two-metal ion mechanism of bovine lens leucine aminopeptidase: active site solvent structure and binding mode of L-leucinal, a gem-diolate transition state analog, by X-ray crystallography. *Biochemistry* **1995**, *34* (45), 14792−14800.
(44) Peters, M. B.; Yang, Y.; Wang, B.; Füsti-Molnár, L.; Weaver, M. N.; Merz, K. M. Structural Survey of Zinc-Containing Proteins and Development of the Zinc AMBER Force Field (ZAFF). *J. Chem. Theory Comput.* **2010**, *6* (9), 2935−2947.
(45) Patel, K.; Kumar, A.; Durani, S. Analysis of the structural consensus of the zinc coordination centers of metalloprotein structures. *Biochim. Biophys. Acta* **2007**, *1774* (10), 1247−1253.
(46) Zhu, M.; Pan, G. Quantum Chemical Studies of Mononuclear Zinc Species of Hydration and Hydrolysis. *J. Phys. Chem. A* **2005**, *109* (33), 7648−7652.

https://doi.org/10.1021/acsomega.3c06139
ACS Omega 2023, 8, 42966−42975